

# PARAMETER ESTIMATION FOR A MARKED POINT PROCESS WITHIN A FRAMEWORK OF MULTIDIMENSIONAL SHAPE EXTRACTION FROM REMOTE SENSING IMAGES

**Saima Ben Hadj, Florent Chatelain, Xavier Descombes and Josiane Zerubia**

Ariana Research Group CNRS/INRIA/UNSA  
 2004, route des Lucioles - BP 93 - 06902 Sophia Antipolis Cedex - FRANCE  
 saima.benhadj@sophia.inria.fr, florent.chatelain@gipsa-lab.inpg.fr, xavier.descombes@sophia.inria.fr, josiane.zerubia@sophia.inria.fr  
 http://www.inria.fr/ariana

**Commission III, WG III/4**

**KEY WORDS:** shape extraction, marked point process, RJMCMC, simulated annealing, SEM.

**ABSTRACT:**

Previously, an estimation method based on the Stochastic Expectation-Maximization algorithm was studied and proved its relevance for estimating the parameters of a marked point process model in order to achieve unsupervised feature extraction from remote sensing images. This method was only applied to a simple model of a marked point process of circles. In this paper, we extend the proposed estimation method to multidimensional shapes such as ellipses and rectangles. Different types of objects have been extracted: flamingos, tree crowns, boats, and building footprints. Furthermore, some prior constraints corresponding to the alignment of boats as well as the alignment of buildings are introduced.

## 1 INTRODUCTION

The problem of feature extraction from remote sensing images has been addressed in several scopes, namely, environment, civilian and military. As the resolution of the provided aerial and satellite images is very high, a smart technique of analysis of such data needs to be developed. In this context, a model of marked point process (Geyer and Møller, 1994, Møller and Waagepetersen, 2004) was previously introduced and proved its suitability to such a problem. It is basically a stochastic model that involves some information about the geometry of the objects present in the image. Certain parameters incorporated in this model must be adjusted automatically, according to the processed image. In this prospect, a study of estimation methods of these parameters proved that a method based on the Stochastic Expectation-Maximization (SEM) algorithm (Celeux et al., 1996) was very relevant. It was firstly validated on a marked point process of circles (Chatelain et al., 2009a, Chatelain et al., 2009b). The aim of this paper is thus to extend this estimation procedure to more general geometrical shapes such as ellipses and rectangles. Several applications will be addressed, namely pink flamingo detection, tree crown extraction, boat detection as well as building outline extraction.

The paper is organized as follows: in the second section, we propose to review the family of marked point processes which has been used to extract surface networks. We then explicit the parameters of our model and describe the proposed estimation method. In the third section, we present the model of an ellipse process. Different tests using the associated estimation procedure have been performed. We discuss the obtained results and we modify the energy model spatially for boat detection. In fact, boats in a seaport are very close and aligned, which makes their discrimination difficult using the model proposed in (Chatelain et al., 2009b). In the following section, we look for the extraction of building outlines which can be represented by a network of rectangles. We therefore expose the adopted rectangle process. Moreover, we propose to append an energy component favoring aligned frames owing that buildings of large cities are usually very organized. Finally we conclude this work by proposing some perspectives.

## 2 PROPOSED MODEL FOR OBJECT EXTRACTION AND PARAMETER ESTIMATION

### 2.1 Proposed model for object extraction

In a marked point process framework (Møller and Waagepetersen, 2004), image features are viewed as a set of objects identified jointly by their position in the image and their geometrical characteristics. Let  $W = \mathcal{P} \times \mathcal{M}$  be the object space. Typically  $W$  is a bounded set of  $\mathbb{R}^d$ , where  $\mathcal{P}$  is the space of the object position while  $\mathcal{M}$  is the space of marks describing the object geometry. A configuration  $\mathbf{x}$  of objects belonging to  $W$  is an unordered set of objects  $\mathbf{x} = \{x_1, \dots, x_n\} \in \Omega_n$ ,  $x_i \in W$ ,  $i = 1, \dots, n$ . A point process  $X$  living in  $W$  is a random variable whose realizations are random configurations of objects in  $\Omega = \bigcup_n \Omega_n$ . In our work, we focus on a particular family of marked point processes, namely the family of Gibbs processes. One major interest of these processes consists in their ability to model the interactions between objects. Denoting by  $\mathbf{y}$  the observed image, the density of the considered marked point process is actually:

$$f_\theta(X = \mathbf{x}|\mathbf{y}) = \frac{e^{-U_\theta(\mathbf{x}, \mathbf{y})}}{c(\theta|\mathbf{y})} \tag{1}$$

where  $c(\theta|\mathbf{y})$  is the normalizing function written in the following form  $\int_\Omega e^{-U_\theta(\mathbf{x}, \mathbf{y})} \mu(d\mathbf{x})$  (where  $\mu(\cdot)$  is the intensity measure of the reference Poisson process).  $\theta$  is a parameter vector, allowing the flexibility of our model and its suitability to several types of images. It hence must be adjusted according to the given image. The process energy  $U_\theta(\mathbf{x}, \mathbf{y})$  is divided into the two types of energies: the external energy,  $U_\theta^e(\mathbf{x}, \mathbf{y})$  which quantifies the fit between the configuration  $\mathbf{x}$  and the data  $\mathbf{y}$  and the internal energy,  $U_\theta^p(\mathbf{x})$  which reflects our prior knowledge about the interactions between objects. Thus, the most likely configuration which allows object extraction corresponds to the global minimum of the total energy:

$$\hat{\mathbf{x}} = \arg \max_{\mathbf{x} \in \Omega} f_\theta(X = \mathbf{x}|\mathbf{y}) = \arg \min_{\mathbf{x} \in \Omega} [U_\theta^e(\mathbf{x}, \mathbf{y}) + U_\theta^p(\mathbf{x})] \tag{2}$$

Algorithmically, the computation of the global minimum of this energy is performed by a simulated annealing scheme (Azencott, 1992).

**2.1.1 Data energy** Two main approaches for computing the data energy term were previously introduced to extract surface networks (Chatelain et al., 2009a). The first one was carried out in a Bayesian framework. Nevertheless, it doesn't sufficiently take into account the morphology of objects. The second one is more efficient. It consists in defining a local energy  $U_\theta^d(u) \in [-1, 1]$  associated with each object  $u$ . Then, the data energy associated with a configuration  $\mathbf{x}$  is proportional to the sum of all the local energies computed on each object  $u$  of  $\mathbf{x}$ :

$$U_\theta^d(\mathbf{x}, \mathbf{y}) = \gamma_d \sum_{u \in \mathbf{x}} U_\theta^d(u, \mathbf{y}) \quad (3)$$

where the parameter  $\gamma_d > 0$  corresponds to the data energy weight. Its definition relies on a contrast measure between the distribution of the set of pixels belonging to an object  $u$  and the distribution of pixels belonging to its border  $\mathcal{F}^\rho(u)$ . The data energy  $U_\theta^d(u)$  is built as a qualification of this contrast measure in order to promote well-placed objects and penalize bad ones:

$$U_\theta^d(u) = \mathcal{Q}\left(\frac{d(u, \mathcal{F}^\rho(u))}{d_0}\right) \quad (4)$$

where  $d(u, \mathcal{F}^\rho(u))$  is the Bhattacharya distance between the object  $u$  and its boundary  $\mathcal{F}^\rho(u)$ .  $\mathcal{Q}_{d_0} : \mathbb{R}^+ \mapsto [-1, 1]$  is a quality function. It attributes a negative value to objects that have a high radiometric distance w.r.t. their border (i.e.  $d(u, \mathcal{F}^\rho(u))$  is above the threshold  $d_0$ ) and a positive value otherwise:

$$\mathcal{Q}(x) = \begin{cases} 1 - x^{1/3} & \text{if } x < 1, \\ \exp\left(-\frac{x-1}{3}\right) - 1 & \text{if } x \geq 1. \end{cases} \quad (5)$$

Using a cubic root in this quality function ensures a moderate penalization when the distance  $d(u, \mathcal{F}^\rho(u))$  is close to the threshold  $d_0$ . To illustrate the behavior of such a function, we give its plot in figure 2(left).

**2.1.2 Prior energy** This energy corresponds to a penalization of the overlapping objects and thus avoids detecting the same object several times. For this purpose, we define the neighborhood system corresponding to overlapping objects by the following relationship:

$$\forall x_i, x_j \in W, x_i \sim x_j \iff \frac{\text{Area}(x_i \cap x_j)}{\min(\text{Area}(x_i), \text{Area}(x_j))} < s \quad (6)$$

The parameter  $s \in [0, 1]$  represents the maximum recovery ratio between two objects. Afterwards, we introduce a "Hard Core" process which penalizes any configuration having at least one overlapping object pair with a recovery rate exceeding a threshold  $s$ . The non-normalized density of such a process is written as follows:  $h_{\beta, \gamma}(\mathbf{x}) = \beta^{n(\mathbf{x})} e^{-U_s(\mathbf{x})}$  where  $\beta$  is the activity parameter,  $n(\mathbf{x})$  is the number of objects in the configuration  $\mathbf{x}$  and  $U_s(\mathbf{x}) = \sum_{1 < i < j < n(\mathbf{x})} t_s(x_i, x_j)$  is the interaction potential of objects in  $\mathbf{x}$ . The interaction function between object pairs  $t_s(x_i, x_j)$  can be written as follows:

$$t_s(x_i, x_j) = \begin{cases} 0 & \text{if } x_i \sim x_j, \\ +\infty & \text{otherwise.} \end{cases} \quad (7)$$

By assigning an infinite energy to object pair that does not interact according to  $\sim$ , the associated probability is practically zero.

## 2.2 Estimation algorithm

Before revealing the proposed estimation method, it is necessary to identify the parameters to be estimated. The parameter vector  $\theta$  embedded in the considered model is composed of: the activity parameter  $\beta$ , the maximal overlapping ratio  $s$ , the data energy weight  $\gamma_d$ , the threshold  $d_0$  involved in the quality function and the width of the boundary of an object  $\rho$ . Some of these parameters can be set in a deterministic way as they have an intuitive interpretation: The boundary width  $\rho$  is usually set to 1 or 2, the threshold  $s$  is set as the tolerated recovery proportion between objects. The previous study of the model parameters has shown that the activity parameter  $\beta$  and the weight parameter  $\gamma_d$  are correlated. The experience proved that a low value of  $\beta$  is compensated by a high value of  $\gamma_d$  and vice versa. Therefore, we decide to estimate only one parameter which is the weight  $\gamma_d$  and set manually the other ones. The problem of parameter estimation consists in identifying the most likely parameter vector  $\theta$  that maximizes the image likelihood  $f_\theta(\mathbf{y})$ . As the density of the observation  $f_\theta(\mathbf{y})$  is unknown, we propose to maximize the extended likelihood  $f_\theta(\mathbf{x}, \mathbf{y})$ . However, the configuration  $\mathbf{x}$  is likewise unknown. The study of estimation methods (Chatelain et al., 2009a) showed that the stochastic version of the Expectation-Maximization (SEM) algorithm (Celeux et al., 1996) is very relevant in such a situation. It consists in iterating the three following steps:

1. **S step:** Simulate a configuration of objects:

$$\mathbf{x}^{(k)} \sim f_{\theta^k}(X/\mathbf{y}) \quad (8)$$

2. **E Step:** Evaluate the extended log-likelihood:

$$Q(\theta, \theta^k; \mathbf{y}) = \log f_\theta(\mathbf{x}^{(k)}, \mathbf{y}) \quad (9)$$

3. **M step:** Maximize the log-likelihood:

$$\theta^{k+1} = \arg \max_{\theta \in \Theta} Q(\theta, \theta^k; \mathbf{y}) \quad (10)$$

Nevertheless, the E step is unreachable as the extended density  $f_\theta(\mathbf{x}^{(k)}, \mathbf{y})$  is not tractable (the normalizing constant is inaccessible). To overcome this difficulty, we propose to approximate the extended likelihood by the pseudo-likelihood (Besag, 1975, Baddeley and Turner, 2000). Its expression in the case of incomplete data is given by:

$$PLW(\theta; \mathbf{x}, \mathbf{y}) = \exp\left(-\int_W \lambda_\theta(u; \mathbf{x}, \mathbf{y}) \Lambda(du)\right) \times \prod_{x_i \in \mathbf{x}} \lambda_\theta(x_i; \mathbf{x}, \mathbf{y}) \quad (11)$$

where  $\lambda_\theta$  is the extended Papangelou intensity which can be written as follows:

$$\lambda_\theta(u; \mathbf{x}, \mathbf{y}) = \beta \exp\left(-\gamma_d U_d(u) - \sum_{x_i \in \mathbf{x}/x_i \neq u} t_s(u, x_i)\right) \quad (12)$$

In practice, the simulation step is performed using a Reversible Jump Metropolis-Hastings algorithm (Green, 1995) or a multiple births and deaths algorithm. Afterwards, the maximization step is performed using the Nelder-Mead Simplex algorithm. The SEM algorithm is supposed to converge when the parameter vector remains stable. Once the parameters are estimated, we determine the most likely object configuration that maximizes the energy model thanks to a simulated annealing algorithm.

### 3 ELLIPSE MODEL

#### 3.1 From circles to ellipses

Firstly, the estimation method was validated for a simple model of marked point process where the objects were circular (Chatelain et al., 2009b). Only one object mark corresponding to the radius of circles was introduced. The simulation results of the proposed approach on a  $274 \times 269$  image of a flamingo colony in Camargue in France were not quite satisfactory (see figure 1). One can

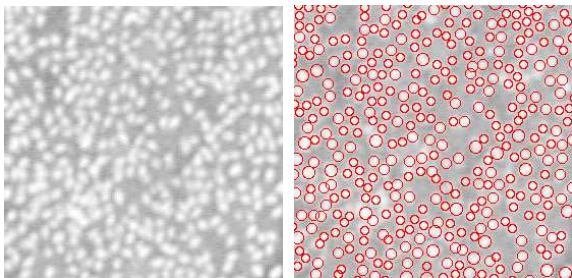


Figure 1: left: flamingo colony in Camargue, France ©Tour de Valat, right: flamingo extraction using a circle model: 363 circles ©INRIA ( $\beta = 1000$ ,  $\gamma_d = 13.88$ ,  $s = 0.3$ ,  $d_0 = 1.33$ ).

notice misdetections on figure 1(right). Thus, such a model does not deal very well with the problem of flamingo extraction. A model of an ellipse process may be more suitable to the flamingo shape. This process is defined on the following object space:

$$W = [0, X_{max}] \times [0, Y_{max}] \times [a_{min}, a_{max}] \times [b_{min}, b_{max}] \times [0, \pi[$$

which corresponds to the parameterization space of an ellipse  $u$  defined by five variables  $u = (x, y, a, b, \omega)$ .  $a_{max}$  and  $a_{min}$  are the parameters that demarcate the space of the semi-major axis  $a$ , and  $b_{max}$  and  $b_{min}$  are the parameters corresponding to the definition domain of the semi-minor axis  $b$ . The figure 2(right) illustrates such a parameterization. This makes the esti-

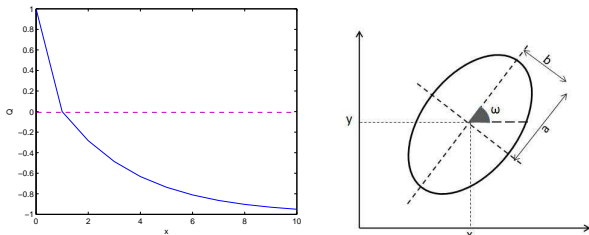


Figure 2: left: quality function, right: ellipse parameterization.

mation algorithm time consuming since the number of parameters is increased using the ellipse process.

#### 3.2 Validation of the ellipse model

In order to validate the proposed estimation method associated with an ellipse process, we tested it on three types of images; the flamingo image considered in the former paragraph, an image of trees in Saone-et-Loire of  $229 \times 196$  pixels (figure 4(left)) and an image of boats of  $385 \times 275$  pixels (figure 5(top)). For each image, we outfaced a new object structure. We manually initialized some parameters. The activity parameter was set as an over-estimation of the number of objects in the image,  $\beta = 1000$  for all the treated images. The maximum overlapping rate was set to  $s = 0.3$ . All our simulations were performed using a processor with  $1.86 GHz$  frequency. The estimation algorithm appears to be computationally expensive. It lasted  $12 min$  for the flamingo

image (see figure 1(left)),  $25 min$  for the tree image (see figure 4(left)) and  $1 h$  and  $36 min$  for the boat image (see figure 5(top)). The set of ellipses obtained at the convergence of the SEM algorithm for the flamingo image is revealed by the figure 3(right). After estimating the data weight, objects are extracted thanks to a simulated annealing algorithm. The estimates as well as the configurations of ellipses corresponding to the flamingo extraction, tree crown extraction and ship detection are respectively depicted in figures 3(right), 4(right) and 5(bottom). These results show that the proposed approach is very relevant for flamingo and tree crown extraction but does not fit the problem of boat detection. Therefore, we suggest in the second paragraph to modify the proposed model for the boat image. Moreover, to assess the accuracy of our solution, we have manually generated the ground truth of the flamingo image: the red ellipses are those that are automatically generated; the black ones are those that are supposed to appear (7 false negatives), the crossed red ellipses correspond to those that are wrongly detected (4 false positives) and all the red ellipses which have a blue point in their midst are considered as correct. From these results we compute the f-measure which is 0.98 and thus we conclude that our solution is very accurate (remark that an error up to 5% is acceptable for ecologists). Besides, the given results are only for one run, the table 1 gives an idea about the computational time average of several runs, the estimate mean  $\bar{\gamma}_d$  and the standard deviation  $E[\gamma_d]$ .

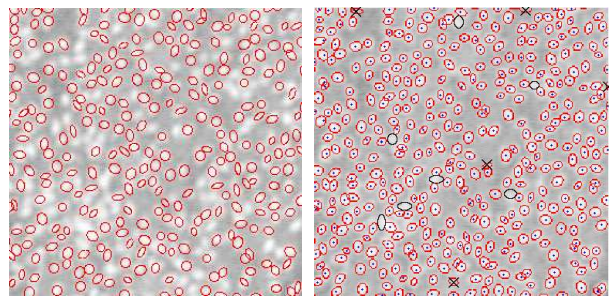


Figure 3: left: simulation step of the SEM algorithm, right: flamingo extraction using an ellipse model 387 ellipses ©INRIA ( $\beta = 1000$ ,  $\gamma_d = 16.25$ ,  $s = 0.3$ ,  $d_0 = 1.33$ )

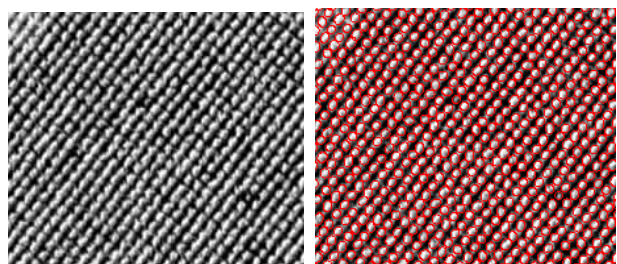


Figure 4: left: plantation in Saone et Loire ©IFN, right: tree crown extraction using an ellipse model: 598 ellipses ©INRIA, ( $\beta = 1000$ ,  $\gamma_d = 15.14$ ,  $s = 0.2$ ,  $d_0 = 2$ ).

	Flamingo image	Tree image	Boat image
Mean time	41 min	24 min	1h and 41 min
$\bar{\gamma}_d$	17.87	14.85	38.62
$E[\gamma_d]$	2.5813	0.5469	0.5427

Table 1: Statistical results

#### 3.3 Modification of the energy model for boat detection

As the boats of the image 5(top) are very close, the border  $\mathcal{F}^\rho(u)$  of an object  $u$  is not homogenous. That is why, we modify its definition and we consider that it corresponds to the two ends of the

circumscribed crown (figure 6(left)). The corresponding SEM algorithm led to the estimate  $\gamma_d = 11.9512$ . The extraction results displayed in figure 7 are enhanced, compared to those of the figure 5(bottom). However, some false-detections corresponding to not aligned ellipses remained. To avoid this problem, we propose to favor close and aligned ellipses. For this purpose, we define an alignment interaction  $\sim_{al}$  between two ellipses (figure 6(right)) as follows:

$$e_1 \sim_{al} e_2 \iff \begin{cases} d_\omega(e_1, e_2) \leq d_{\omega_{max}} \\ d_\alpha(e_1, e_2) \leq d_{\alpha_{max}} \\ d_C(e_1, e_2) \leq d_{C_{max}} \end{cases} \quad (13)$$

where  $d_\omega(e_1, e_2) = |\omega_1 - \omega_2|$  is the difference of the orientation of ellipses  $e_1$  and  $e_2$ , and  $d_\alpha(e_1, e_2) = \left| \alpha - \left( \frac{\omega_1 + \omega_2}{2} + \frac{\pi}{2} \right) \right|$  is a measure that checks that the ellipses are not shifted. Finally,  $d_C(e_1, e_2) = |d(c_1, c_2) - (b_1 + b_2)|$ , where  $d(c_1, c_2)$  stands for the Euclidian distance between the centers  $c_1$  and  $c_2$  of the two ellipses  $e_1$  and  $e_2$  respectively. Then, we append a prior energy that promotes two tangent ellipses as follows:

$$U_{al}(e_1, e_2) = \begin{cases} \delta(d_C(e_1, e_2), d_{C_{max}}) \cdot \\ \varpi(d_\alpha(e_1, e_2), d_{\alpha_{max}}) & \text{if } e_1 \sim_{al} e_2, \\ 0 & \text{otherwise.} \end{cases} \quad (14)$$

where  $\varpi(x, x_{max})$  is a reward function, previously introduced in (Ortner et al., 2008) to favor aligned buildings:

$$\varpi(x, x_{max}) = -\frac{1}{x_{max}^2} \left[ \frac{1 + x_{max}^2}{1 + x^2} - 1 \right], \quad \forall x \leq x_{max} \quad (15)$$

It is negative, when the measure  $x$  is below the threshold  $x_{max}$  and zero, if the measure  $x$  equals  $x_{max}$ . The weight  $\delta$  is dependent on the distance between ellipses. It equals 1, when the ellipses are too close and is close to zero, otherwise. Finally, the prior energy of a configuration  $\mathbf{x}$ , which corresponds to the alignment constraint is the sum over all the object pairs of the

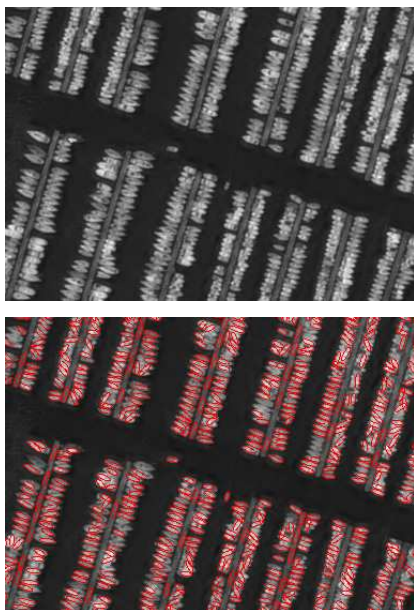


Figure 5: top: photograph of vessels in France ©CNES, bottom: boat detection using an ellipse model 508 ellipses ©INRIA ( $\beta = 1000$ ,  $\gamma_d = 38.65$ ,  $s = 0.3$ ,  $d_0 = 6$ ).

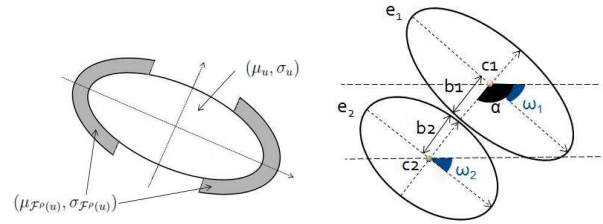


Figure 6: left: new definition of the ellipse border, right: tangent ellipses

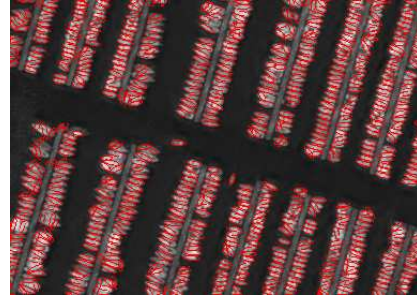


Figure 7: Extraction results with modification of the data term: 635 ellipses ( $\beta = 1000$ ,  $\gamma_d = 11.95$ ,  $s = 0.3$ ,  $d_0 = 6$ ).

configuration  $\mathbf{x}$ :

$$U_{al}^p(\mathbf{x}) = \gamma_{al} \sum_{1 < i < j < n(\mathbf{x})} U_{al}(e_i, e_j) \quad (16)$$

The weight  $\gamma_{al}$  is likewise a parameter of our model and must be estimated by the SEM algorithm. The experience showed that a value of  $\gamma_{al}$  lower than  $\gamma_d$  leads to good results for boat detection. In our simulations, the initial value  $\gamma_{al}^0$  used in the SEM algorithm for the parameter  $\gamma_{al}$  is set to  $\gamma_{al}^0 = \gamma_d^0 / 3$ , where  $\gamma_d^0$  is the initial value for  $\gamma_d$  (see (Chatelain et al., 2009b) for more details on the numerical evaluation of  $\gamma_d^0$ ). The estimation procedure converges after 1 h and 38 min and provides the following estimates:  $\gamma_d = 25.3426$  and  $\gamma_{al} = 10.535$ . The extraction results depicted in figure 8 show that the ellipses are better organized. However,

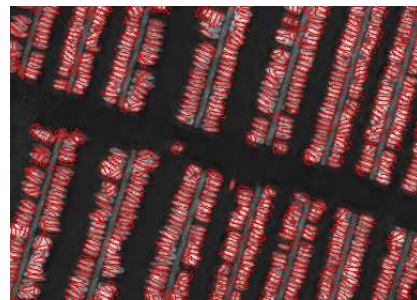


Figure 8: Extraction results with an alignment constraint between ellipses: 715 ellipses ( $\beta = 1000$ ,  $\gamma_d = 25.34$ ,  $\gamma_{al} = 10.53$ ,  $s = 0.3$ ,  $d_0 = 6$ ).

one can notice some false-detections standing for aligned ellipses that are placed on the same boat (the number of boats automatically estimated is 715 while the hand-counted number of boats is 570). Furthermore, introducing a repulsive energy that penalizes not aligned ellipses does not enhance boat extraction results and leads to several misdetections. Thus, in a similar way to (Perrin et al., 2005), we propose to promote aligned ellipses that have a particular orientation (which is denoted by  $\omega_N$ ), since the ships of

the processed image have a common direction. Thus, we modify the expression of the energy related to the alignment interactions of an object  $e$  as follows:

$$U_{al\omega}(e) = \begin{cases} U_{al}^p(\mathbf{x} \cup \{e\}) - U_{al}^p(\mathbf{x}) & \text{if } |\omega_e - \omega_N| \leq d_{\omega_{max}} \\ 0 & \text{otherwise} \end{cases} \quad (17)$$

In order to validate this idea, we empirically define the boat direction and we then simulate the SEM algorithm corresponding to such a model. The estimates  $\gamma_d = 27.56$  and  $\gamma_{al} = 9.18$  contribute to the detection of 523 boats depicted in figure 9. The de-



Figure 9: Extraction results favoring aligned ellipses having a particular direction: 523 ellipses ( $\beta = 1000$ ,  $\gamma_d = 27.56$ ,  $\gamma_{al} = 9.18$ ,  $s = 0.3$ ,  $d_0 = 6$ ).

tection results are greatly improved. Nevertheless, this approach is not useful when the boats do not have a common direction. In this case, locally assessing the boat direction is a possible alternative.

## 4 RECTANGLE MODEL

### 4.1 From ellipses to rectangles

In this section, we are interested in a marked point process which is defined in the following state space (a bounded set of  $\mathbb{R}^5$ ):

$$W = \mathcal{P} \times \mathcal{M} = [1, X_{max}] \times [1, Y_{max}] \times [l_{min}, l_{max}] \times [L_{min}, L_{max}] \times [0, \pi[$$

where  $(l_{min}, l_{max})$  respectively stands for the minimum and the maximum semi-width of the rectangle,  $(L_{min}, L_{max})$  are the minimum and the maximum of its semi-length and  $\omega \in [0, \pi[$  is its orientation. This parameterization is illustrated in figure 11(left).

### 4.2 Validation of the rectangle model

We simulate the estimation procedure associated with the described rectangle model on the Digital Elevation Model (DEM) of a part of Amiens image of  $231 \times 194$  pixels, depicted on figure 10(left). Moreover, our tests were performed with the same CPU used in the previous simulations (a processor with 1.86 GHz frequency). The estimate  $\gamma_d = 29.402$  contributes to the configuration displayed in figure 10(right), obtained at the extraction phase. Some rectangle pairs are not close enough and not very well aligned which could account for some misdetections. To overcome this problem, we propose to promote close and aligned rectangles.

### 4.3 Modification of the energy model for building outline detection

We propose to introduce an energy term that favors aligned and close frames. We thus use a similar component to that involved

in (Ortner et al., 2008). We define two different relationships between building features; actually alignment and orthogonal interactions. In fact, orthogonal interaction is not viewed as a simple rotation between two interacted frames since some constraints on their appropriate edges must be taken into account as it will be explained later.

**4.3.1 Alignment interaction** We say that the rectangle  $u$  is aligned with the rectangle  $v$ , if one of its short edges is opposite to one short edge of the second rectangle  $v$  (figure 11(middle)). In other words, they are close enough such that the Euclidian distance  $d_C(i, j)$  between the corner  $i$  of the rectangle  $u$  and the corner  $j$  of the rectangle  $v$  is low and their appropriate short edges are opposite ( $i + j = 3$ ) as well as they have almost the same orientation such that their angle difference (modulo  $\pi$ )  $d_\omega(u, v)$  is low enough:

$$u \sim_{al_i} v, \quad \forall i \in \{0, 1, 2, 3\} \iff \begin{cases} d_C(i, j) \leq d_{C_m} \\ d_\omega(u, v) \leq d_{\omega_m} \\ i + j = 3 \end{cases} \quad (18)$$

Hence, the prior energy dealing with the alignment constraint is built such that it attributes a negative value to the pair of objects which exhibits jointly a low distance between their appropriate extremities and a low angle difference:

$$U_{al_i}(u, v) = \begin{cases} \frac{1}{2} \varpi(d_C(i, j), d_{C_m}) + \frac{1}{2} \varpi(d_\omega(u, v), d_{\omega_m}) & \text{if } u \sim_{al_i} v \\ 0 & \text{otherwise} \end{cases} \quad (19)$$

where  $\varpi(x, x_{max})$  is a reward function given by equation (15). Summing all the local energies over the object pairs of the configuration  $\mathbf{x}$ , we actually obtain the alignment energy of the configuration  $\mathbf{x}$ :

$$U_{al}(\mathbf{x}) = \gamma_{al} \sum_{1 < j < k < n(\mathbf{x})} \sum_{0 \leq i \leq 3} U_{al_i}(x_j, x_k) \quad (20)$$

where  $\gamma_{al}$  is a regularization parameter that corresponds to the alignment energy.

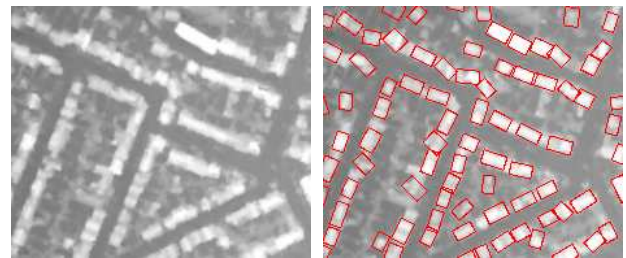


Figure 10: left: DEM of a part of Amiens ©IGN, right: building outline extraction using a rectangle model: 83 rectangles ©INRIA, ( $\beta = 500$ ,  $\gamma_d = 29.402$ ,  $s = 0.2$ ,  $d_0 = 4$ ).

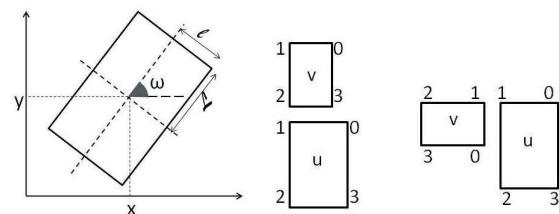


Figure 11: left: rectangle parameterization, middle: aligned rectangles, right: orthogonal rectangles.

**4.3.2 Orthogonal connection** We propose to promote likewise orthogonal frames. In fact, two rectangles are said orthogonal, if one rectangle short side is opposite to the other rectangle long side (figure 11(right)). That means, they satisfy the following conditions:

$$u \sim_{orth_i} v, \forall i \in \{0, 1, 2, 3\} \iff \begin{cases} d_C(i, j) \leq d_{C_m} \\ |d_\omega(u, v) - \frac{\pi}{2}| \leq d_{\omega_m} \\ i + j = 0, 2, 4 \text{ or } 6 \end{cases} \quad (21)$$

By analogy with the expression (19) and (20), we define an energy component of a configuration  $\mathbf{x}$ , related to orthogonal connections  $\sim_{orth_i}$  as follows:

$$U_{orth}(\mathbf{x}) = \gamma_{orth} \sum_{1 < j < k < n(\mathbf{x})} \sum_{0 \leq i \leq 3} U_{orth_i}(x_j, x_k)$$

where  $\gamma_{orth}$  is the weight of the described energy. Having specified the different types of connections that link buildings of an urban area, we can define an energy term that summarizes all the interactions between rectangles representing buildings as follows:

$$U_{\theta_{int}}^p(\mathbf{x}) = \gamma_{int} [U_{al}^p(\mathbf{x}) + U_{orth}^p(\mathbf{x})] \quad (22)$$

A new parameter  $\gamma_{int}$  related to rectangle interactions is introduced in order to offset the value of the other parameters  $\gamma_{al}$  and  $\gamma_{orth}$  which can be set to 1, since both alignment and orthogonal connections are present in an equitable manner in the image 10(left). Hence, we are interested in estimating only one interaction parameter which is the weight  $\gamma_{int}$ , by the SEM algorithm. Moreover, we initialize this interaction weight to  $\gamma_{int}^0 = \gamma_d^0/2$ , since the empirical test showed that it must have a lower value than that of the data energy weight  $\gamma_d$ . The SEM estimation algorithm performed on the part of Amiens considered in the former test is very slow. It required 6 h and 21 min and contributed to the following estimates  $\gamma_d = 30.0599$  and  $\gamma_{int} = 16.8494$ . The result of the extraction phase depicted in figure 12 shows that the frames are closer and more aligned than those of the previous simulation. However, some pairs are still distant. In fact, the dis-

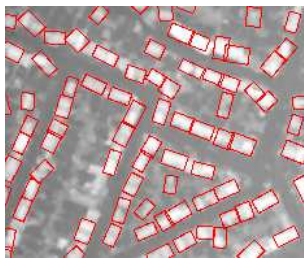


Figure 12: Extraction results, favoring orthogonal and aligned rectangles: 83 rectangles ( $\beta = 1000$ ,  $\gamma_d = 30.05$ ,  $\gamma_{int} = 16.84$ ,  $s = 0.3$ ,  $d_0 = 4$ ).

tance between two remote objects cannot support a new object without overlapping with them. To avoid such a case, we can increase the tolerated recovery rate  $s$  or we can employ object with variable size allowing the presence of small and large rectangles. In fact, in our tests we have limited the size of the occurred rectangles when we have set the object space parameters.

## 5 CONCLUSION AND FUTURE WORK

In this paper, we generalized the estimation method associated with a marked point process model to the case of multidimensional shapes such as ellipses and rectangles. The proposed estimation method is based on the SEM algorithm. It showed its

interest for estimating the parameters of an ellipse process within the framework of flamingo and tree crown extraction. Its application to an image of boats in a seaport required the modification of both the data energy and the prior energy components of the proposed model. Moreover, in order to extract building footprint in a dense urban area, we introduced an energy term providing orthogonal and aligned frames. For that matter, we estimated by the SEM algorithm a new parameter related to this type of interaction. Nevertheless, incorporating ellipse or rectangle process in an iterative algorithm such as SEM algorithm is time consuming. Accelerating the proposed algorithm by optimization strategies could be a nice future work. The computation of the pseudo-likelihood, representing more than 70% of the computation, could be parallelized using a multi-threaded program. Besides, the direction of boats involved in the prior term was set manually. It could be interesting to estimate it automatically.

## ACKNOWLEDGEMENTS

The authors would like to thank the French Space Agency (CNES), the French Forest Inventory (IFN) and Tour du Valat for providing the images presented in this paper. This research work has been partially supported by INRIA through a post-doctoral grant for the second author and partially by CNES through a contract.

## REFERENCES

- Azencott, R., 1992. Simulated annealing: Parallelization techniques. Wiley, NY, Springer-Verlag.
- Baddeley, A. and Turner, R., 2000. Practical maximum pseudo-likelihood for spatial point patterns. Australian and New Zealand Journal of Statistics 42(3), pp. 283–322.
- Besag, J., 1975. Statistical analysis of non-lattice data. The Statistician 24(3), pp. 179–195.
- Celeux, G., Chauveau, D. and Diebolt, J., 1996. Stochastic versions of the EM algorithm: An experimental study in the mixture case. Journal of Statistical Computation and Simulation 55(4), pp. 287–314.
- Chatelain, F., Descombes, X. and Zerubia, J., 2009a. Estimation des paramètres de processus ponctuels marqués dans le cadre de l'extraction d'objets en imagerie de télédétection. In: GRETSI'09, Dijon, France.
- Chatelain, F., Descombes, X. and Zerubia, J., 2009b. Parameter estimation for marked point processes. Application to object extraction from remote sensing images. In: EMMCVPR'09, Springer-Verlag, Berlin, Heidelberg, pp. 221–234.
- Geyer, C. and Møller, J., 1994. Simulation procedures and likelihood inference for spatial point processes. Scandinavian Journal of Statistics 21(4), pp. 359–373.
- Green, P., 1995. Reversible jump Markov chain Monte Carlo computation and Bayesian model determination. Biometrika 82(4), pp. 711–732.
- Møller, J. and Waagepetersen, R., 2004. Statistical inference and simulation for spatial point processes. CRC Press.
- Ortner, M., Descombes, X. and Zerubia, J., 2008. A marked point process of rectangles and segments for automatic analysis of Digital Elevation Models. IEEE Transactions on Pattern Analysis and Machine Intelligence 30(1), pp. 105–119.
- Perrin, G., Descombes, X. and Zerubia, J., 2005. A Marked Point Process Model for Tree Crown Extraction in Plantations. In: Proc. IEEE International Conference on Image Processing (ICIP), Genoa.